

Article

## An Experimental Study on Non-Compression X-Bracing Systems Using Carbon Fiber Composite Cable for Seismic Strengthening of RC Buildings

Kang Seok Lee

School of Architecture, Chonnam National University, Gwangju, 500-757, Korea;  
E-Mail: [kslnist@jnu.ac.kr](mailto:kslnist@jnu.ac.kr); Tel.: +82-62-530-1645; Fax: +82-62-530-1630

Academic Editors: Alper Ilki and Masoud Motavalli

Received: 22 May 2015 / Accepted: 31 August 2015 / Published: 9 September 2015

**Abstract:** Cross-bracing (X-bracing) is one of the most popular methods of seismic retrofitting, and has been shown to significantly increase the structural stiffness and strength of buildings. Conventional steel X-bracing methods typically exhibit brittle failure at the connection between the brace and the building, or buckling failure of the braces. This study investigated the structural properties of a new type of non-compression X-bracing system using carbon fiber composite cable (CFCC). This non-compression X-bracing system uses CFCC bracing and bolt connections between structural members and the terminal fixer of the CFCC, instead of conventional steel bracing. The aim is to overcome the brittle and buckling failures that can occur at the connection and bracings with conventional steel X-bracing methods. We carried out cyclic loading tests, and the maximum load carrying capacity and deformation were investigated, as well as hysteresis in the lateral load–drift relations. The test results revealed that the CFCC X-bracing system installed in reinforced concrete frames enhanced the strength markedly, and buckling failure of the bracing was not observed.

**Keywords:** carbon fiber composite cable; X-bracing; reinforced concrete; reinforcement; seismic strengthening; seismic capacity

### 1. Introduction

Existing earthquake-resistance methods focus primarily on encasing reinforced concrete (RC) columns using steel or fiber composite materials. A number of reports over the past two decades have shown that the most efficient strengthening method to resist the lateral earthquake loads for RC buildings

is to use steel bracing, and retrofitted steel bracing can strengthen earthquake-damaged buildings and increase the seismic capacity of existing RC buildings [1–7].

Viswanath *et al.* [8] analytically showed that X-bracing significantly increases the structural stiffness of buildings, and reduces the maximum inter-story drift. Triangulated- and X-bracing systems have been used in five-story RC buildings, without considering seismic design, and a significant strengthening effect was found [9]. Scale tests for seven-story RC buildings reinforced using steel bracing have been reported, and an enhancement of vertical and horizontal resistance was found just prior to buckling failure of the bracing in response to earthquake loadings [10]. An RC school building was strengthened using post-tensioned rod braces, which increased the moment capacity rather than increasing the ductility [11]. Direct connection has been shown to exhibit favorable earthquake resistance compared with indirect connection [1,12–15].

Seismic reinforcement using steel braces typically exhibits brittle failure at the connections or buckling failure of the braces. There have been a number of reports of methods to address the buckling failure of the braces. These have mostly focused on the buckling restrained braced (BRB) system. An analytical study to calculate the confidence parameters of buckling failure of a four-story steel office building was carried out, and indicated that carefully assessing the braced steel frames was particularly important, especially to prevent collapse [16].

In Japan, BRB frames have become increasingly popular because of the favorable earthquake resistance [17]. A new type of bidirectional-resistant ductile end diaphragm using BRB for applications in bridges was introduced [18]. A BRB device encased in steel tubing and mortar has been reported [19], and the authors found effective performance in response to cyclic loading. A buckling restrained braced frame (BRBF) with a pinned moment connection has been reported, favorable performance in mitigating residual drift, soft-story deformation, and preventing undesirable failure modes in the beam-column connection, and was analyzed using nonlinear dynamic analysis [20]. A nine-story building reinforced with a special concentrically braced frame (SCBF), a buckling restrained braced frame (BRBF) and a mega-braced frame (MBF) was simulated to evaluate the seismic performance of these different bracing configurations. The MBF series exhibited the most effective resistance to lateral drift, even though it was relatively low-weight [21]. A method to inhibit buckling failure of the braces has been reported, which uses non-compression braces installed with sliding equipment at the brace connection [22].

Recently, Ju *et al.* [23] reported a technique for non-compression X-bracing systems using carbon fiber anchors for seismic strengthening of RC structures. A carbon fiber is a bundle of yarn-type carbon. Using cyclic load tests, they verified that the carbon fiber anchors have advantages compared with conventional steel X-bracing systems, including an improved strength-to-weight ratio of carbon fiber, compression-free bracing, and confinement using carbon fiber sheets at the brittle concrete-steel joint area. They also reported that further work is needed to optimize details of the connection between the carbon fiber bracing and columns.

In this paper, we describe a new technique for non-compression X-bracing using carbon fiber composite cable (CFCC) for seismic strengthening of RC structures. This CFCC X-bracing system consists of CFCC bracing and bolt connections between the structural members and the terminal fixer of the CFCC, rather than the conventional X-bracing system, which is commonly used with steel bracing. We report the seismic performance of an RC frame reinforced with CFCC X-bracing using cyclic loading

tests, and the maximum load carrying capacity and deformation were characterized, as well as hysteresis of the lateral load–drift relation.

## 2. Seismic Strengthening Using CFCC X-Bracing

### 2.1. CFCC

Tokyo Rope [24] developed CFCC, a structural reinforcing cable, formed of carbon fibers and thermosetting resins with a polyester skin, and using a new composite technology to create a stranded cable. Thus, the structural behavior of CFCC is similar to that of carbon fiber strands, which has no plastic behavior.

Figure 1 shows optical images of the CFCC, including the terminal fixer. CFCC exploits the excellent mechanical properties of carbon fiber, and exhibits a high tensile strength (approximately equal to that of steel strands for prestressed concrete, as discussed later), a high tensile modulus (similar to that of steel strands for prestressed concrete), is lightweight (approximately one-fifth the mass of steel strands), has good corrosion resistance (high acid and alkali resistance), is non-magnetic, flexible (the stranded configuration of the cables allows them to be easily coiled), and a low linear expansion rate (the coefficient of linear expansion is approximately 1/20 of that of steel).

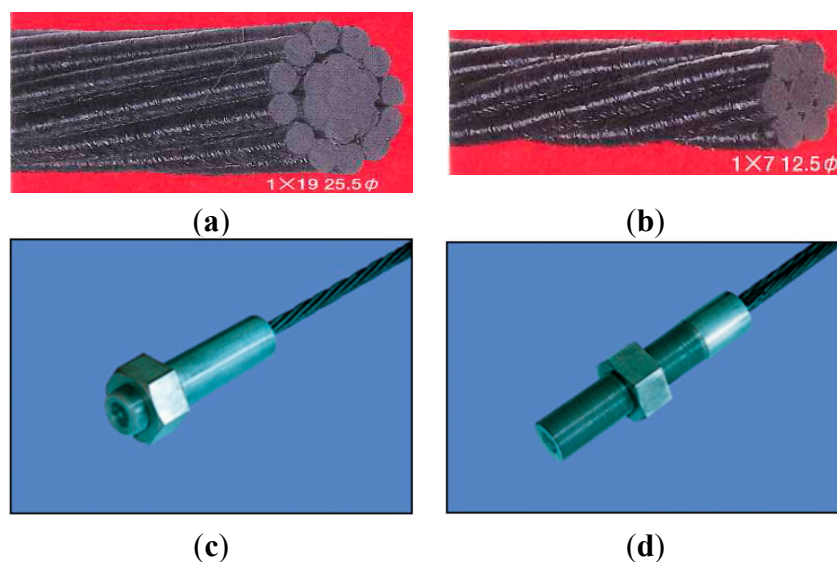


**Figure 1.** Optical images of standard CFCC (Tokyo Rope, [24]): (a) 19-strand, 25.5 mm diameter and (b) seven-strand, 12.5 mm diameter; (c) A terminal fixer for a single cable made by expansive material filling method (ES-type) and (d) a terminal fixer for multiple cables (EM-type). Reprinted with permission from reference [24]. Copyright 2013, Tokyo Rope.

Figure 2 shows the load-elongation characteristics of standard CFCC, as well as those of steel strand for prestressed concrete and aramid fiber reinforced plastic (AFRP) [24]. The tensile modulus of CFCC is approximately twice that of AFRP, and approximately equal to that of steel strand for prestressed concrete. CFCC has a high tensile modulus, which is similar to that of steel strand for prestressed concrete. Table 1 lists the material properties of standard CFCC. The tensile elastic modulus of the

standard CFCC is in the range 130–160 kN/mm<sup>2</sup>. As will be described later, the ultimate load at failure of seven-strand CFCC with a diameter of 15.2 mm, used in this study, is 270 kN.

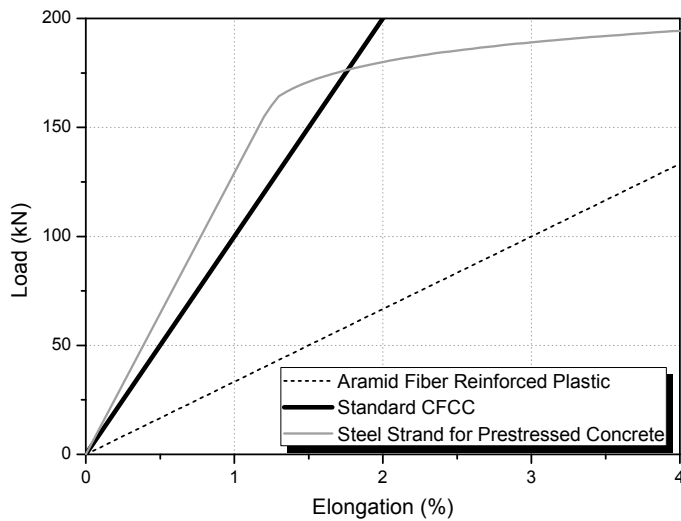


**Figure 2.** Load–elongation relations of standard carbon fiber composite cable (CFCC) (Tokyo Rope, [24] 2013). Reprinted with permission from reference [24]. Copyright 2013, Tokyo Rope.

CFCC reinforcement has been used mainly in the field of civil engineering, including tendons in pre-stressed concrete bridges, cantilever cables and external cables of the pre-stressed concrete bridges, tendons of the ground anchors, and stay cables for strengthening the catwalks of bridges [24]. CFCC reinforcement techniques for buildings have not yet been investigated. In this study, we describe for the first time the technique of X-bracing using CFCC for seismic reinforcement of RC buildings.

**Table 1.** Specification of the standard CFCC cables.

Configuration and diameter <sup>a</sup>	Diameter $\varphi$ (mm)	Effective cross section <sup>b</sup> (mm <sup>2</sup> )	Tensile strength at break (kN)	Nominal mass density (g/m)	Tensile elastic modulus (kN/mm <sup>2</sup> )
U, 5.0 $\varphi$	5.0	15.2	38	30	167
1 × 7, 7.5 $\varphi$	7.5	31.1	76	60	155
1 × 7, 10.5 $\varphi$	10.5	57.8	141	111	155
1 × 7, 12.5 $\varphi$	12.5	76.0	184	145	155
1 × 7, 15.2 $\varphi$	15.2	115.6	270	221	155
1 × 7, 17.2 $\varphi$	17.2	151.1	350	289	155
1 × 19, 20.5 $\varphi$	20.5	206.2	316	410	137
1 × 19, 25.5 $\varphi$	25.5	304.7	467	606	137
1 × 19, 28.5 $\varphi$	28.5	401.0	594	777	137
1 × 37, 35.5 $\varphi$	35.5	591.2	841	1,185	127
1 × 37, 40.0 $\varphi$	40.0	798.7	1,200	1,529	145

<sup>a</sup> U is the abbreviation of uni-,  $\varphi$  shows the diameter, and 1 × 7, 1 × 19, and 1 × 37 are a cable formed with 7, 19, and 37 strands, respectively. <sup>b</sup> Effective cross section is defined as the cross sectional area of composite materials, *i.e.*, carbon fibers and thermosetting resins, excepting the polyester skin.

## 2.2. CFCC X-Bracing

The CFCC X-bracing system for RC buildings consists of flat-plate and protrusion configurations, as shown in Figure 3. Following coring 30-mm-diameter holes in the existing beam, steel devices for connecting of the flat-plate and protrusion-type reinforcements were mechanically installed using prestressing steel bars through the holes at both edges of the beam. The CFCC was cross-braced using a terminal fixer, as shown in Figure 3c, and bolted to steel connecting devices. The flat-plate and protrusion type CFCC X-bracing systems use a bolt-nut connection method, which enables control over the deflection of the bracing.

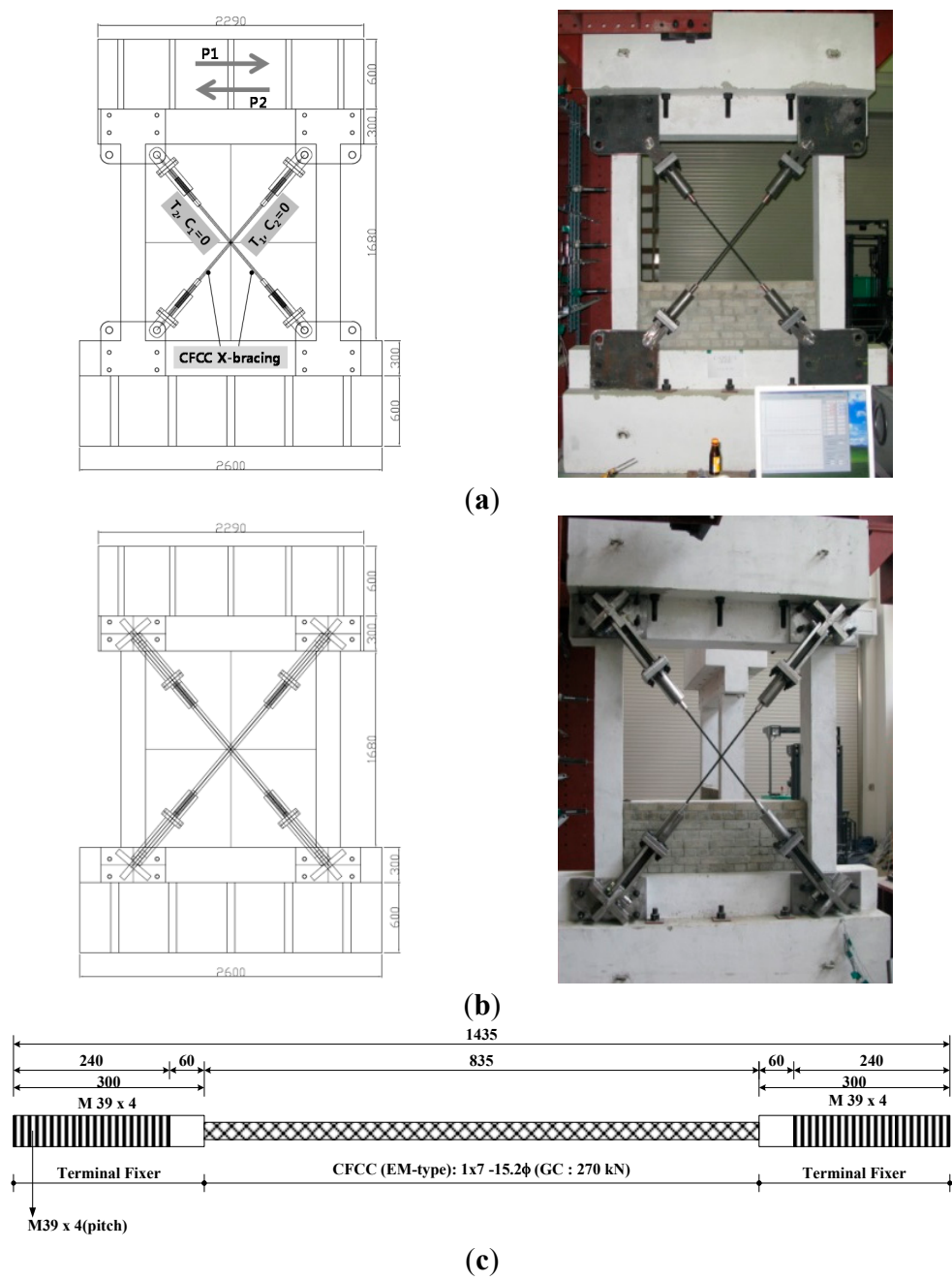


**Figure 3.** Seismic reinforcement methods using CFCC X-Bracing: **(a)** Flat-plate and **(b)** protrusion configurations. **(c)** Details of an individual CFCC reinforcement.

The structural behavior of the CFCC X-bracing is indicated in Figure 3a. When a lateral force acts, as shown by P1, the ascending brace experiences a tensile force  $T_1$  and the descending brace has no compressive force; *i.e.*,  $C_1 = 0$ . For a lateral force P2, the descending brace has a tensile force  $T_2$  and the ascending brace has no compressive force, so  $C_2 = 0$ . There is no compressive stress on the CFCC X-bracing system in response to lateral loading.

### 3. Structural Tests

#### 3.1. Material Characteristics of Concrete, Steel Rebar and CFCC

The specified compressive strength of the concrete used in the tests was 24 MPa. The results of cylindrical compressive tests were 19.0 MPa for 14 days and 24.3 MPa for 28 days, as listed in Table 2. The specified yield strength of the steel reinforcing bar (rebar) used in the test specimens was 400 MPa. Two diameters of rebar were used: D13 for the main rebar of the column and D6 for the hoop. The tensile strength of steel rebar from using a universal testing machine (UTM) was  $567.2 \pm 8.2$  MPa for D13 and  $538.0 \pm 3.0$  MPa for D6.

**Table 2.** Material properties of the concrete.

Specified strength (MPa)	Compressive strength (MPa)	
	14 days	28 days
24	19.3	23.1
	18.3	19.9
	19.4	29.9
Average	19.0	24.3

The properties of the  $1 \times 7$ , 15.2 φ used here are listed in Table 1. We used a terminal fixer for multiple cables (EM). The diameter of the CFCC was φ = 15.2 mm, the effective cross section was  $115.6 \text{ mm}^2$ , the tensile strength at break was 270 kN, the nominal mass density was 221 g/m, and the tensile elastic modulus was  $155 \text{ kN/mm}^2$ .

#### 3.2. Design, Variables and Fabrication of Test Specimens

Specimens were designed based on the frame of a typical Korean school building [25], and fabricated for cyclic load tests to investigate the reinforcement properties of the CFCC X-bracing system. The building was a three-story RC structure designed in the 1980s, without seismic reinforcement. The structure consisted of RC frames with spandrel brick walls in the longitudinal direction, and in-filled brick walls in the transverse direction. One span of the exterior frame in the longitudinal direction corresponds to columns, the beam and the spandrel brick wall, as shown in Figure 3. This was selected for the tests because the seismic capacity in the transverse direction with the in-filled brick walls is higher than that in the longitudinal direction [26].

Three types of specimen were designed and fabricated for the experimental tests: a control test specimen (not reinforced), as shown in Figure 4, a test specimen reinforced with CFCC X-bracing using the flat-plate, as shown in Figure 3a, and a test specimen strengthened with the CFCC X-bracing using the protrusion configuration, as shown in Figure 3b. Table 3 lists details of each of the specimens.

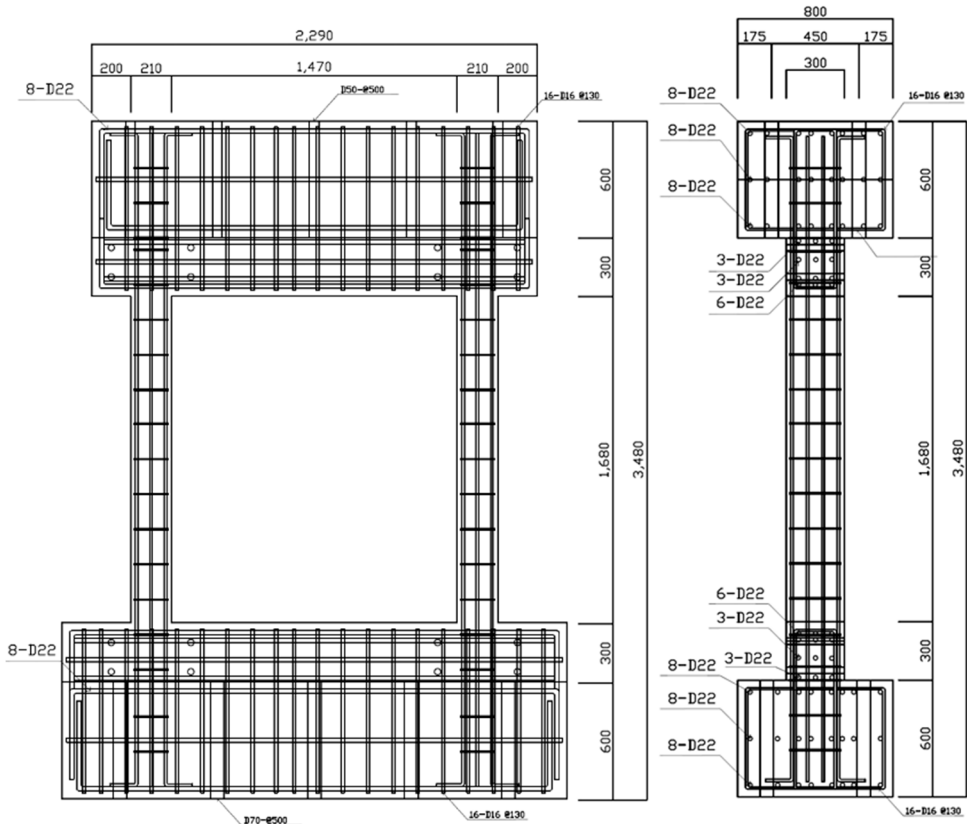


**Figure 4.** Details of the control specimen.

**Table 3.** Summary of the specimens used in this study. RCFR: Control specimen without CFCC X-bracing; CFCC-1: CFCC X-bracing (flat-plate); CFCC-2: CFCC X-bracing (protrusion).

Specimens	Column clear height, $h_0$ (mm)	Column depth, $D$ (mm)	$h_0/D$	Strengthening material	Strengthening types	Connection method
RCFR	1680	210	6.72	-	-	-
CFCC-1	1680	210	6.72	CFCC 1 × 7, 15.2 φ	Flat-plate	Bolt-nut system
CFCC-2	1680	210	6.72	CFCC 1 × 7, 15.2 φ	Protrusion	Bolt-nut system

All specimens had identical dimensions and arrangements of rebar. The cross-section of the columns was  $210 \times 300$  mm, and the ratio of column clear height to the depth  $h_0/D = 6.72$ . Each specimen was prepared with 10-D13 type SD40 main rebar, reinforced with shear reinforcement D6 steel bars at 180-mm intervals. Beams were fabricated to install the CFCC X-bracing, which were designed to have same behavior with a stub at the top, as shown in Figure 4. The stub, with a high stiffness, was installed at the top of each specimen to provide confinement for the columns. The spandrel brick wall was 480 mm high, and constructed using B-type brick; *i.e.*, 190 mm long, 90 mm wide and 57 mm thick. The compressive strength of the brick was 8 MPa.

### 3.3. Testing Procedure

The main purpose of the tests was to investigate the seismic resistance of the non-compression CFCC X-bracing in terms of the maximum load-carrying capacity, deformation, and hysteresis of the lateral load–drift relations.

Figure 5 shows the test set-up for cyclic loading test. Loads were applied using two actuators with a capacity of 300 kN, and one actuator with a capacity of 500 kN. The two columns were subjected to a constant vertical load of 219 kN during cyclic lateral loading using the two 300-kN actuators. The cyclic lateral loading was controlled by the lateral displacement of the 500-kN actuator.

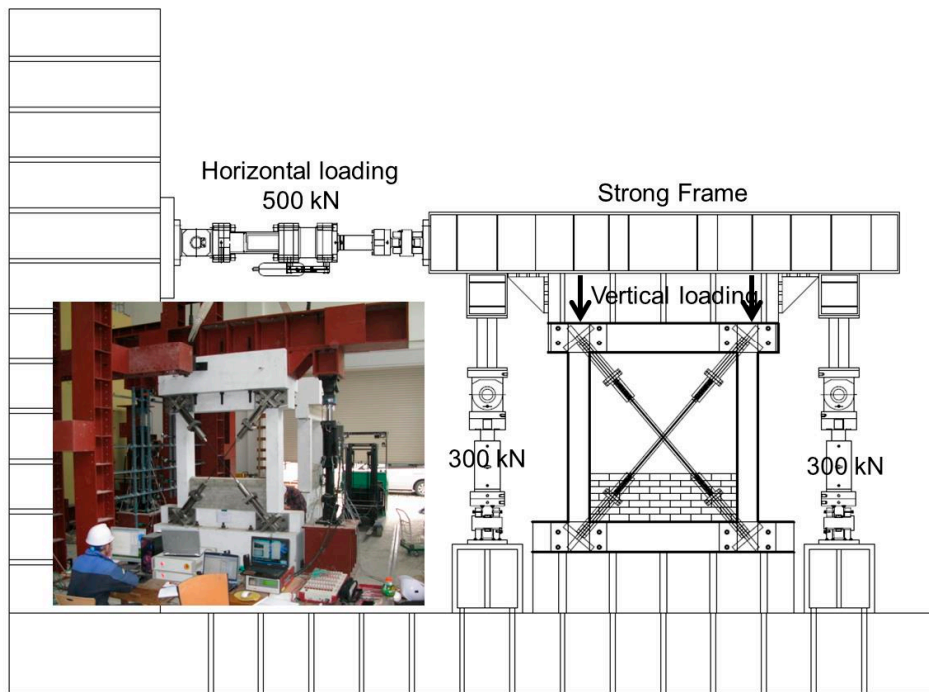


**Figure 5.** Experimental configuration for the cyclic loading tests.

The load cycles were repeated three times at the lateral drift angles ( $R$ ) of 0.08%, 0.1%, 0.12%, 0.15%, 0.2%, 0.25%, 0.31%, 0.4%, 0.49%, 0.62%, 0.79%, 1%, 1.24%, 1.54%, 2%, and 3.33%. Then, at each loading step, the lateral drift angle ( $R$ ) was increased to approximately 1.2 times of the previous one, repeating the load cycle three times. Table 4 lists the loading cycles applied to the each specimen.

**Table 4.** The loading cycles used in the experiments.

Loading step	1	2	3	4	5	6	7	8
Loading cycles	1–3	4–6	7–9	10–12	13–15	16–18	19–21	22–24
Drift angle $R$ (%)	0.08	0.1	0.12	0.15	0.2	0.25	0.31	0.4
Lateral drift $\delta$ (mm)	1.34	1.68	2.10	2.63	3.36	4.2	5.25	6.72
Loading step	9	10	11	12	13	14	15	16
Loading cycles	25–27	28–30	31–33	34–36	37–39	40–42	43–45	46–48
Drift angle $R$ (%)	0.49	0.62	0.79	1	1.24	1.54	2	3.33
Lateral drift $\delta$ (mm)	8.4	10.5	13.4	16.8	21	26.3	33.6	56

#### 4. Failure Sequence and Lateral Load–Drift Curves

For all specimens, the compressive behavior of the CFCC X-bracing was out-of-plane. This was originally expected to be compression-free, so that buckling failure of the braces would not occur. The behavior of the control and CFCC X-bracing strengthened specimens differed significantly. The flat

plate-type and the protrusion-type specimens exhibited similar evidence of failure, with a similar crack appearance, and load–drift relations; however, the CFCC X-bracing specimens did not exhibit damage resulting from tensile stress. In the following discussion, we focus on the crack and failure patterns in terms of the lateral drift and load–drift relations during the final stages of the test. Each loading step was identical during the three loading cycles. Table 5 lists the test results of the mechanical characterization following different loading steps, and Table 6 lists the maximum shear strengths and drifts for the three specimens.

**Table 5.** Results of the mechanical loading tests for the specimens.

Specimens	Load (kN)	Drift (mm)	Drift angle R (%)	Observation
RCFR	37	2.6	0.15	Flexural cracks
	68	5.3	0.31	Shear cracks
	−65	−5.3	0.31	Shear cracks
	96	10.5	0.62	Shear cracks > 3 mm in width
	148	26.3	1.54	Large shear cracks and peeling of concrete cover
	163	32.9	2.0	Ultimate state
	99	44.0	2.6	Shear collapse
CFCC-1	29	1.7	0.1	Flexural cracks
	46	2.6	0.15	Shear cracks
	263	33	1.96	Ultimate state
	−228	31.2	1.8	Shear failure
CFCC-2	−40	1.34	0.08	Flexural cracks
	65	2.6	0.15	Shear cracks
	−293	32.3	1.92	Ultimate state
	−241	33	1.96	Shear failure

**Table 6.** The maximum strengths and drifts of the specimens.

Specimens	Positive		Negative		Final failure mode
	$V_{\max}$ <sup>a</sup> (kN)	$\delta_{\max}$ <sup>b</sup> (mm)	$V_{\max}$ <sup>a</sup> (kN)	$\delta_{\max}$ <sup>b</sup> (mm)	
RCFR	163	32.9	−160	−33.6	Shear failure and collapse of the columns
CFCC-1	263	33	−257	−26.2	Shear failure of the columns
CFCC-2	275	31.2	−293	−32.3	Shear failure of the columns

<sup>a</sup>  $V_{\max}$ : Maximum shear strength; <sup>b</sup>  $\delta_{\max}$ : Drift at the maximum point.

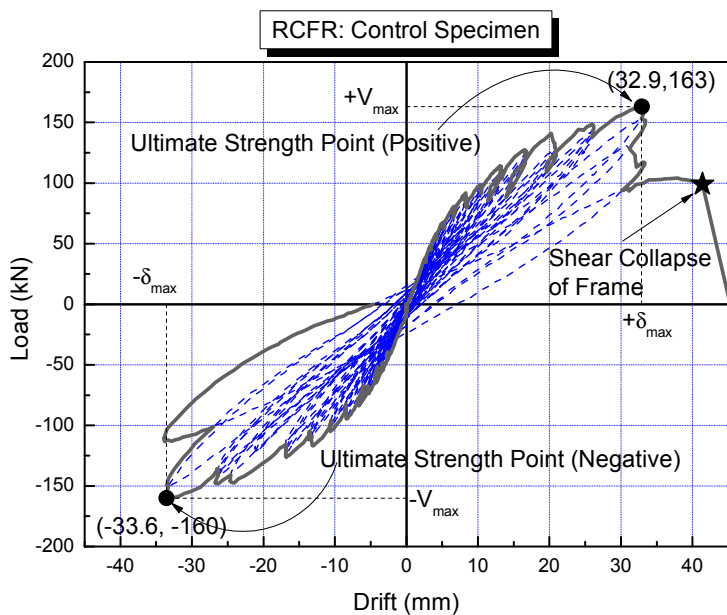
#### 4.1. Unbraced Control Specimen (RCFR)

Figure 6 shows the RCFR specimen following the final cyclic load test, and Figure 7 shows load–drift curves for the RCFR specimen. The first observed crack occurred at a positive load of 37 kN, and a small flexural crack appeared in the bottom column faces after three cycles at the fourth loading step ( $R = 0.15\%$ ). Cracking was not observed in the center of the column. Flexural cracks extended into the middle of the column after step four. Following the seventh loading step ( $R = 0.31\%$ ), with a load of both positive 68 kN and negative −65 kN, shear cracks were observed at the top faces of the columns, and a number of diagonal shear cracks appeared, some of which were more than 3 mm wide. When the applied load reached 148 kN, at the fourteenth positive loading step ( $R = 1.54\%$ ), more large shear cracks

were observed, with increased widths. We observed peeling failure due to shear forces from the concrete cover. This is likely to be the result of insufficient shear confinement.



**Figure 6.** The RCFR specimen following the cyclic loading test.



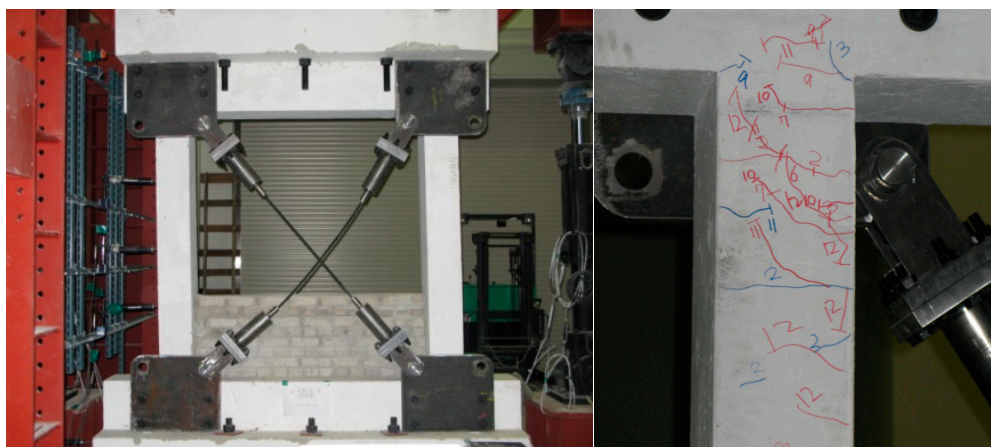
**Figure 7.** Load–drift relations for the RCFR sample.

Shear collapse occurred at the top of both columns following the application of a load of 99 kN, with a lateral drift of 44.0 mm ( $R = 2.6\%$ ). The maximum load capacity of the frame of the RCFR specimen was a positive load of 163 kN, with a lateral drift of 32.9 mm ( $R = 2.0\%$ ) (Table 6). The maximum positive load capacity was similar to the maximum negative load capacity of 160 kN, with a lateral drift of 33.6 mm.

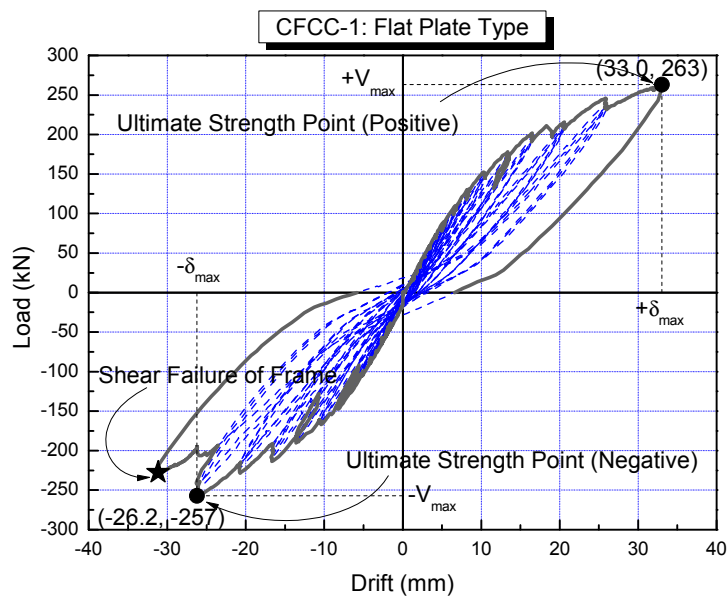
#### 4.2. Flat-Plate Specimen (CFCC-1)

Figure 8 shows a photograph of the CFCC-1 specimen following the cyclic loading test, and Figure 9 shows the load–drift curves. The CFCC-1 specimen had the flat-plate type X-bracing system (Figure 3a). Cracks first appeared with a positive load of 29 kN, and a small flexural crack appeared in the top

and bottom column faces following two cycles of the second loading step ( $R = 0.1\%$ ). The flexural cracks increased in number and width, and shear cracks appeared following the fourth loading step ( $R = 0.15\%$ ), with a positive load of 46 kN; these shear cracks extended into the middle of both columns. The maximum load capacity of the CFCC-1 specimen was a positive load of 263 kN, with a lateral drift of 33 mm ( $R = 1.96\%$ ) (Table 6 and Figure 9). Shear failure occurred at the top and bottom of both columns under a negative load of 228 kN, with a lateral drift of 31.2 mm ( $R = 1.8\%$ ), as shown in Figure 9. It should be noted that buckling failure of the CFCC X-bracing was not observed. The CFCC X-bracing system for RC frames was therefore an effective reinforcement technique that can markedly increase the shear strength.



**Figure 8.** The CFCC-1 specimen following the cyclic loading tests.



**Figure 9.** Load–drift relations for sample CFCC-1.

#### 4.3. Protrusion-Type Specimen (CFCC-2)

Figure 10 shows a photograph of the CFCC-2 sample following the cyclic loading tests, and Figure 11 shows load–drift curves. The CFCC-2 test specimen was reinforced using the protrusion-type X-bracing system, as shown in Figure 3b. The first crack was observed with a negative load of  $-40$  kN and with

a lateral drift of 1.34 mm. This was a slight flexural crack, which appeared in the top and bottom of the column faces after three cycles of the first loading step ( $R = 0.08\%$ ). Flexural cracks also appeared following the second and third loading steps, and shear cracks appeared following the fourth loading step ( $R = 0.15\%$ ) with a positive load of 65 kN. The shear cracks increased in number and extended into the middle of both columns following the fourth loading step. Compared with the control specimen, however, there were a small number of cracks, which were less wide.

The maximum load capacity of specimen CFCC-2 was a negative load of  $-293$  kN with a lateral drift of 32.3 mm ( $R = 1.92\%$ ) (Table 6 and Figure 11), which is similar to specimen CFCC-1. Shear failure occurred at the top and bottom of both columns, and bucking failure was not observed.

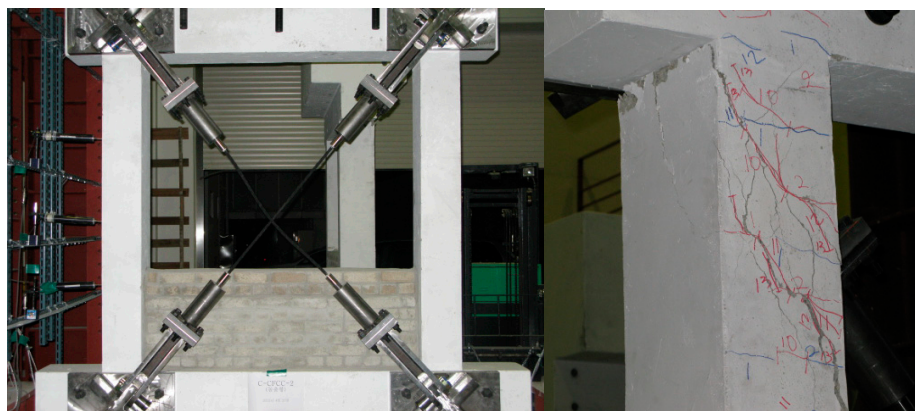


**Figure 10.** The CFCC-2 specimen following the cyclic load tests.

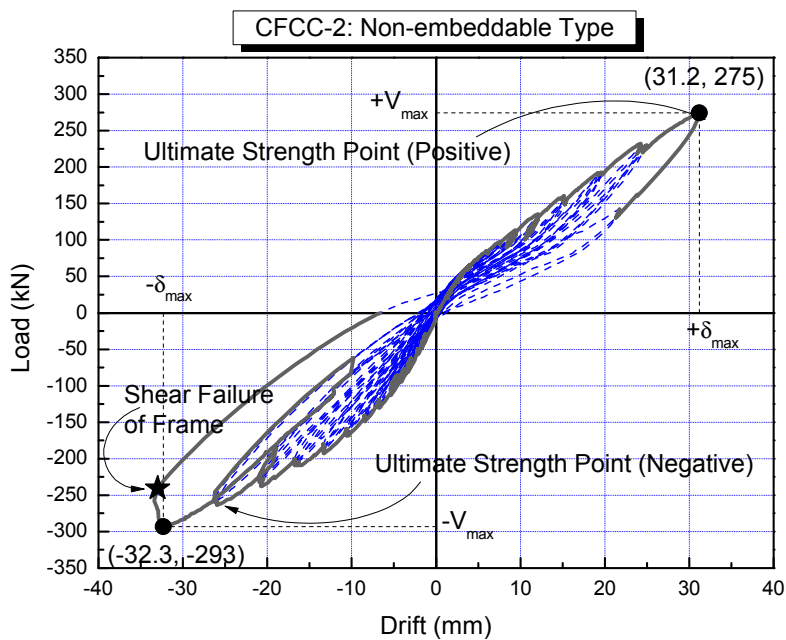


**Figure 11.** Load–drift relation for the CFCC-2 specimen.

## 5. Strength and Deformation

Figure 12 shows envelop curves of the lateral load–drift relations for the RCFR, CFCC-1 and CFCC-2 specimens. The larger of the maximum positive and negative load values were used here (see Figures 7, 9 and 11). Table 7 lists maximum strength and deformation capacities. The strength

ratio (SR) is defined as the ratio of maximum load  $V_{\max}$  of specimens with the CFCC X-bracing to that of the RCFR control specimen, and the drift ratio (DR) indicates the ratio of drift at the maximum point  $\delta_{\max}$  of the specimens with the CFCC X-bracing to that of the RCFR control specimen.

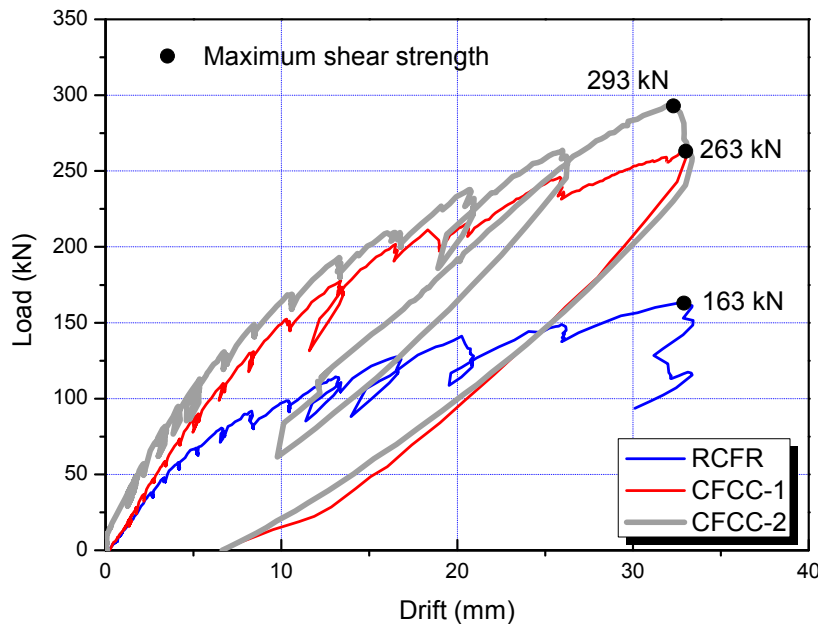


**Figure 12.** The envelope of the load–drift relations of the three specimens.

**Table 7.** Summary of the strengths and deformation capacities.

Specimen	Maximum shear strength $V_{\max}$ (kN) <sup>a</sup>	Drift at the maximum point $\delta_{\max}$ (mm)	Strength ratio (SR) <sup>b</sup>	Drift ratio (DR) <sup>c</sup>
RCFR	163	32.9	1.00 (163/163)	1.00 (32.9/32.9)
CFCC-1	263 (61.3%)	33.0	1.61 (263/163)	1.00 (33/32.9)
CFCC-2	293 (79.8%)	32.3	1.80 (293/163)	0.98 (32.3/32.9)

<sup>a</sup> Data in parentheses indicate a strengthening effect in terms of shear strength compared with the RCFR control specimen; <sup>b</sup> SR is the ratio of maximum load  $V_{\max}$  of specimens strengthened with CFCC to that of the RCFR control specimen; <sup>c</sup> DR is the ratio of the drift at the maximum point  $\delta_{\max}$  of specimens strengthened with CFCC to that of the RCFR control specimen.

The maximum shear strength of specimens CFCC-1 was 263 kN, and that of CFCC-2 was 293 kN; this represents an increase of a factor of approximately 1.6–1.8 (*i.e.*, 60%–80%) larger than the RCFR control specimen (where the maximum shear strength was 163 kN). The drift ratio (DR) of the CFCC X-braced specimens was approximately 1.0, which means that the maximum drift was similar to that of the control RCFR specimen. This is because the failure modes of three specimens were similar; *i.e.*, shear failure for the CFCC X-braced specimens and shear collapse of both columns for the RCFR control specimen.

The results of strength and deformation capacities mentioned above show that the CFCC X-bracing system for RC frames is an effective retrofitting technique to provide increased strength, which is the most promising approach for low- to medium-rise RC buildings. If the ductility is insufficient, an adequate strength can reduce the inelastic displacement [27].

## 6. Conclusion

We have investigated the structural properties of CFCC X-bracing systems designed to improve the earthquake resistance of RC structures using cyclic loading tests. The CFCC X-bracing system proposed here has numerous advantages compared with conventional steel X-bracing systems, including an improved strength-to-weight ratio of the CFCC, compression-free bracing, and connection using bolt-nut joints, which can control the deflection of the X-bracing. These structural properties enable enhanced seismic resistance of RC frames. The results of this investigation can be summarized as follows.

The control RCFR specimen reached maximum load capacity at positive and negative loads of approximately 160 kN, with a lateral drift of 33 mm ( $R = 2.0\%$ ). Shear collapse occurred at the top of both columns under a load of 99 kN, with a lateral drift of 44.0 mm ( $R = 2.6\%$ ). The frame of a typical Korean RC school building was selected for designing the RCFR specimen, which represents a shear failure mode. The building was a three-story RC structure designed in the 1980s without seismic resistance features.

The maximum load capacity of specimen CFCC-1, which was reinforced with CFCC X-bracing with a flat plate-type configuration, was a positive load of 263 kN, with a lateral drift of 33 mm ( $R = 1.96\%$ ). The CFCC-2 specimen, with the protrusion-type X-bracing configuration exhibited a maximum strength with a negative load of  $-293$  kN with a lateral drift of 32.3 mm ( $R = 1.92\%$ ), which is similar to that of specimen CFCC-1. Both of the CFCC X-braced system exhibited shear failure modes at the top and bottom of both columns, buckling failure of the bracing was not observed.

The strength capacity of both CFCC-1 and CFCC-2 specimens increased by a factor of approximately 1.7 compared with that of the RCFR control specimen. The deformation capacity of the CFCC X-braced specimens, however, was approximately equal to that of the RCFR control specimen. These strength and deformation capacities indicate that the CFCC X-bracing system is an effective retrofitting technique to provide increased strength. The reinforcement effect depends on the bracing material. It follows that the target strength capacity can be designed by choosing the appropriate CFCC X-bracing system.

This approach to seismic strengthening can eliminate the buckling failure modes of conventional steel X-bracing systems. However, further work is required to optimize the details of the connection between the CFCC bracing and the columns or beams, as well as to design the seismic retrofitting procedures for existing RC buildings.

This research was a preliminary approach regarding the use of new braces in carbon fibers and focused on an experimental investigation to study applicability of a new type of non-compression CFCC X-bracing system proposed in this study. As a recommendation for future work, however, additional theoretical and analytical studies are needed to justify the seismic behavior of the proposed CFCC X-bracing system.

## Acknowledgments

This work was supported by National Research Foundation of Korea grant 2013R1A1A2009761, funded by the Ministry of Education, Korea.

## Conflicts of Interest

The author declares no conflict of interest.

## References

1. Maher, M.R.; Kousari, R.; Razazan, M. Pushover tests on steel X-braced and knee-braced RC frames. *Eng. Struct.* **2003**, *25*, 1697–1705. [[CrossRef](#)]
2. Badoux, M.; Jirsa, J. Steel bracing of RC frames for seismic retrofitting. *J. Struct. Eng.* **1990**, *116*, 55–74. [[CrossRef](#)]
3. Calderon, V.E.; Foutch, A.; Hjelmstad, K.D.; Figueroa-Gutierrez, E.; Tena-Colunga, A. Seismic Retrofit of a RC Building: A Case Study. In Proceedings of the Ninth World Conference on Earthquake Engineering, Tokyo-Kyoto, Japan, 2–9 August 1988; pp. 451–456.
4. Foti, D. Response of frames seismically protected with passive systems in near-field areas. *Int. J. Struct. Eng.* **2014**, *5*, 326–345. [[CrossRef](#)]
5. Mazza, F.; Vulcano, A. Control of the earthquake and wind dynamic response of steel-framed buildings by using additional braces and/or viscoelastic dampers. *Earthq. Eng. Struct. Dyn.* **2011**, *40*, 155–174. [[CrossRef](#)]
6. Sorace, S.; Terenzi, G. Dissipative bracing-based seismic retrofit of R/C school buildings. *Open Constr. Build. Technol. J.* **2012**, *6*, 334–345. [[CrossRef](#)]
7. Foti, D.; Bozzo, L.; López-Almansa, F. Numerical efficiency assessment of energy dissipators for seismic protection of buildings. *Earthq. Eng. Struct. Dyn.* **1998**, *27*, 543–556. [[CrossRef](#)]
8. Viswanath, K.G.; Prakash, K.B.; Desai, A. Seismic analysis of steel braced reinforced concrete frames. *Int. J. Civ. Struct. Eng.* **2010**, *1*, 114–122.
9. Nateghi-A, F. Seismic strengthening of eightstorey RC apartment building using steel braces. *Eng. Struct.* **1995**, *17*, 455–461. [[CrossRef](#)]
10. Jones, E.A.; Jirsa, J.O. *Seismic Strengthening of a Reinforced Concrete Frame Using Structural Steel Bracing*; Report for a Research Project of National Science Foundation: Arlington County, VA, USA; May; 1986.
11. Hwang, S.J.; Chiou, T.C.; Hsiao, F.P.; Chiou, Y.J.; Alcocer, S.M. Field test of RC school building retrofitted by post-tensioned rods. In Proceedings of the 14th World Conference on Earthquake Engineering, Beijing, China, 12–17 October 2008.
12. Maher, M.R.; Sahebi, A. Experimental investigation on the use of steel bracing in reinforced concrete frames. In Proceedings of the Second International Conference on Seismic and Earthquake Engineering, Iran; 1995; pp. 775–784.
13. Maher, M.R.; Sahebi, A. Use of steel bracing in reinforced concrete frames. *Eng. Struct.* **1997**, *19*, 1018–1024. [[CrossRef](#)]
14. Abou-Elfath, H.; Ghobarah, A. Behaviour of reinforced concrete frames rehabilitated with concentric steel bracing. *Can. J. Civ. Eng.* **2000**, *27*, 433–444. [[CrossRef](#)]
15. Ghobarah, A.; Abou Elfath, H. Rehabilitation of a reinforced concrete frame using eccentric steel bracing. *Eng. Struct.* **2001**, *23*, 745–755. [[CrossRef](#)]

16. Chang, H.Y.; Chiu, C.K. Performance assessment of buckling restrained braces. *Proced. Eng.* **2011**, *14*, 2187–2195. [[CrossRef](#)]
17. Xie, Q. State of the art of buckling-restrained braces in Asia. *J. Constr. Steel Res.* **2005**, *61*, 727–748. [[CrossRef](#)]
18. Celik, O.C.; Bruneau, M. Seismic behavior of bidirectional-resistant ductile end diaphragms with buckling restrained braces in straight steel bridges. *Eng. Struct.* **2009**, *31*, 380–393. [[CrossRef](#)]
19. Palazzo, G.; López-Almansa, F.; Cahís, X.; Crisafulli, F. A low-tech dissipative buckling restrained brace. Design, analysis, production and testing. *Eng. Struct.* **2009**, *31*, 2152–2161. [[CrossRef](#)]
20. Ariyaratana, C.; Fahnestock, L.A. Evaluation of buckling-restrained braced frame seismic performance considering reserve strength. *Eng. Struct.* **2011**, *33*, 77–89. [[CrossRef](#)]
21. Di Sarno, L.; Elnashai, A.S. Bracing systems for seismic retrofitting of steel frames. *J. Constr. Steel Res.* **2009**, *65*, 452–465. [[CrossRef](#)]
22. Tamai, H.; Takamatsu, T. Cyclic loading tests on a non-compression brace considering performance-based seismic design. *J. Constr. Steel Res.* **2005**, *61*, 1301–1317. [[CrossRef](#)]
23. Ju, M.; Lee, K.S.; Sim, J.; Kwon, H. Non-compression X-bracing system using CF anchors for seismic strengthening of RC structures. *Mag. Concr. Res.* **2014**, *66*, 159–174. [[CrossRef](#)]
24. Tokyo Rope MFG. Co., Ltd. *Catalogue of CFCC-Carbon Fiber Composite Cable*; Tokyo, Japan, 2013.
25. Lee, K.S.; Shin, S.W. A new methodology for performance-based seismic evaluation of low-rise reinforced concrete buildings using nonlinear required strengths. *J. Adv. Concr. Technol.* **2013**, *11*, 151–166. [[CrossRef](#)]
26. Federal Emergency Management Agency (FEMA). *FEMA 310 Handbook for Seismic Evaluation of Buildings—A Prestandard*; Washington, D.C., WA, USA, 1998.
27. Japan Building Disaster Prevention Association (JBDA). English Version: Standard for Seismic Evaluation of Existing Reinforced Concrete Buildings, Guidelines for Seismic Retrofit of Existing Reinforced Concrete Buildings, and Technical Manual for Seismic Evaluation and Seismic Retrofit of Existing Reinforced Concrete Buildings. Tokyo, Japan, 2005.

© 2015 by the author; licensee MDPI, Basel, Switzerland. This article is an open access article distributed under the terms and conditions of the Creative Commons Attribution license (<http://creativecommons.org/licenses/by/4.0/>).